

REPORT DOCUMENTATION PAGE			<i>Form Approved</i> OMB No. 0704-0188	
Public reporting burden for this collection of information is estimated to average 1 hour per response, including the time for reviewing instructions, searching existing data sources, gathering and maintaining the data needed, and completing and reviewing this collection of information. Send comments regarding this burden estimate or any other aspect of this collection of information, including suggestions for reducing this burden to Department of Defense, Washington Headquarters Services, Directorate for Information Operations and Reports (0704-0188), 1215 Jefferson Davis Highway, Suite 1204, Arlington, VA 22202-4302. Respondents should be aware that notwithstanding any other provision of law, no person shall be subject to any penalty for failing to comply with a collection of information if it does not display a currently valid OMB control number. PLEASE DO NOT RETURN YOUR FORM TO THE ABOVE ADDRESS.				
1. REPORT DATE (DD-MM-YYYY) 28-09-2010		2. REPORT TYPE Article		3. DATES COVERED (From - To) SEPT 2010 - OCT 2010
4. TITLE AND SUBTITLE FlyEyes: A CCD-based wavefront sensor for PUEO, the CFHT curvature AO system			5a. CONTRACT NUMBER FA8720-05-C-0002	
			5b. GRANT NUMBER	
			5c. PROGRAM ELEMENT NUMBER	
6. AUTHOR(S) Olivier Lai, Jean-Charles Cuillandre, Kevin K.Y. Ho, Marc Baril, Tom Benedict, Jeff Ward, Jim Thomas, Derrick Salmon, Chueh-Jen Lin, Shiang-Yu Wang, Gerry Luppino, Reinhold Dorn, Pascal Puget, Barry Burke, and James Beletic			5d. PROJECT NUMBER	
			5e. TASK NUMBER	
			5f. WORK UNIT NUMBER	
7. PERFORMING ORGANIZATION NAME(S) AND ADDRESS(ES) MIT Lincoln Laboratory 244 Wood Street Lexington, MA 02420			8. PERFORMING ORGANIZATION REPORT NUMBER	
9. SPONSORING / MONITORING AGENCY NAME(S) AND ADDRESS(ES) Univ. of Hawaii/Inst. for Astronomy 2680 Woodlawn Dr. Honolulu, HI 96822			10. SPONSOR/MONITOR'S ACRONYM(S) UHI/IFA	
			11. SPONSOR/MONITOR'S REPORT NUMBER(S)	
12. DISTRIBUTION / AVAILABILITY STATEMENT DISTRIBUTION STATEMENT A. Approved for public release; distribution is unlimited.				
13. SUPPLEMENTARY NOTES				
14. ABSTRACT Adaptive optics wavefront sensing imposes stringent requirements on detectors due to the simultaneous need for extremely low read noise and high frame rates. Curvature wavefront sensing measurements are based on the normalized intensity of the signal in a given subaperture and Avalanche Photo Diodes (APDs) have traditionally been used as detectors in curvature systems such as the Canada France Hawaii Telescope (CFHT) Adaptive Optics (AO) Bonnette, called PUEO after the endemic Hawaiian owl. Passively quenched APDs are robust but have low QE (~40%), while actively quenched APDs can have much higher QE, but have been known to fail. Furthermore, curvature systems with large numbers of subapertures are now in operation and the cost of individual APDs may become prohibitive for such systems. Thus a CCD-based alternative appears very attractive, and development of a specific chip was initiated at ESO ten years ago. In this paper, we report on the performance of the FlyEyes camera, a project which was conceived to compare the performance of the backside-illuminated custom-designed CCD detector with an array of APDs, used in an operational and well-characterized curvature wavefront AO system. The on-sky performance is demonstrated to be unaffected on bright guide stars (i.e. negligible latency) and although the faint end suffers from the 2.5 e- read noise, the performance can be regained by lowering the frame rate on the wavefront sensor. In this paper, we report on results that show that the CCD can be used to replace an array of expensive APDs. This would enable to cost-effectively upgrade PUEO to a higher order system, as has been proposed at various occasions.				
15. SUBJECT TERMS wavefront sensing, adaptive optics, CCD				
16. SECURITY CLASSIFICATION OF: U			17. LIMITATION OF ABSTRACT SAR	18. NUMBER OF PAGES 32
a. REPORT U	b. ABSTRACT U	c. THIS PAGE U		
				19b. TELEPHONE NUMBER (include area code) 781-981-5997

JA-17544

CRDA APPROVAL

2/28/200

**FlyEyes: A CCD-based wavefront sensor for PUEO, the CFHT
curvature AO system**

Olivier Lai, Jean-Charles Cuillandre, Kevin K.Y. Ho, Marc Baril, Tom Benedict, Jeff
Ward, Jim Thomas, Derrick Salmon

Canada France Hawaii Telescope, 65-1238 Mamalahoa Hwy, Kamuela, HI 96743, USA.

Chueh-Jen Lin, Shiang-Yu Wang

Institute for Astronomy and Astrophysics, National Taiwan University, Taipei, Taiwan,
R.O.C.

Gerry Luppino

GL Scientific, 3367 Waialae avenue, Honolulu, Hawaii 96816 USA

Reinhold Dorn

European Southern Observatory, Garching bei Munchen, Germany

Pascal Puget

Laboratoire d'Astrophysique de l'Observatoire de Grenoble, Grenoble, France

Barry Burke

MIT Lincoln Laboratory, Lexington, MA, USA

and

James Beletic

Teledyne Imaging Sensors, Camarillo, CA 93102

Received _____; accepted _____

**The MIT Lincoln Lab portion of this work was performed under a Collaboration Agreement between MIT Lincoln Laboratory and The University of Hawaii, Institute for Astronomy (IfA). Opinions, interpretations, conclusions, and recommendations are those of the authors, and do not necessarily represent the view of the United States Government.*

ABSTRACT

Adaptive optics wavefront sensing imposes stringent requirements on detectors due to the simultaneous need for extremely low read noise and high frame rates. Curvature wavefront sensing measurements are based on the normalized intensity of the signal in a given subaperture and Avalanche Photo Diodes (APDs) have traditionally been used as detectors in curvature systems such as the Canada France Hawaii Telescope (CFHT) Adaptive Optics (AO) Bonnette, called PUEO after the endemic Hawaiian owl. Passively quenched APDs are robust but have low QE ($\sim 40\%$), while actively quenched APDs can have much higher QE, but have been known to fail. Furthermore, curvature systems with large numbers of subapertures are now in operation and the cost of individual APDs may become prohibitive for such systems. Thus a CCD-based alternative appears very attractive, and development of a specific chip was initiated at ESO ten years ago. In this paper, we report on the performance of the FlyEyes camera, a project which was conceived to compare the performance of the backside-illuminated custom-designed CCD detector with an array of APDs, used in an operational and well-characterized curvature wavefront AO system. The on-sky performance is demonstrated to be unaffected on bright guide stars (i.e. negligible latency) and although the faint end suffers from the $2.5\ e^-$ read noise, the performance can be regained by lowering the frame rate on the wavefront sensor. In this paper, we report on results that show that the CCD can be used to replace an array of expensive APDs. This would enable to cost-effectively upgrade PUEO to a higher order system, as has been proposed at various occasions.

Subject headings: wavefront sensing, adaptive optics, CCD.

1. Introduction

Curvature wavefront-sensing adaptive optics systems continue to be used and developed with excellent results at many facilities; e.g. MACAO, SINFONI, CRIRES at ESO, NICI at Gemini and C-188 at Subaru (see e.g. Racine 2006). A clear advantage of curvature wavefront sensing is its normalized intensity measurement scheme, which allows single pixel photon counting detectors within each subaperture and avoids the need to generate and measure an image, using complex optics as in a Shack-Hartmann wavefront sensor. Avalanche Photo Diodes (APDs) have traditionally been used as detectors for curvature WFS, but their quantum efficiency (on the order of 40% for passively quenched APDs), their cost and failure rate (particularly for actively quenched APDs), suggests that developing a CCD based detector for curvature sensing would be a useful endeavor. CFHT was eager to test such a system in anticipation that its user community should decide to upgrade its current AO system PUEO (Lai et al. 2003; Lai 2004). This led to the development of the FlyEyes detector which consists of two fiber-fed MIT Lincoln Laboratory CCID-35 CCD arrays inside a dewar, and was intended for direct comparison with the APDs in PUEO as a swappable unit (Cuillandre et al. 2003; Ho et al. 2004, 2006). This paper describes the final system as integrated in PUEO and the results of on-sky testing. The remainder of this section describes the CFHT AO system, PUEO and the CCID-35 detector. Section 2 describes the FlyEyes camera, its implementation and the goals of the FlyEyes project. Simulations to estimate the expected performance and study the modes of operations of FlyEyes in different flux levels are presented in section 3 and section 4 contains the results of on-sky results and comparison to the APDs. Section 5 concludes by summarizing and outlining the potential use of the FlyEyes detector.

1.1. PUEO

The CFHT adaptive optics system, PUEO, has been in service since first light in 1996 and continues to see routine usage. A full description of PUEO and its performance can be found in Rigaut et al. (1998). PUEO is based on curvature wavefront sensing with a 19-element bimorph deformable mirror (DM) and 19 passively quenched APDs. Light from the wavefront is divided into 19 sub-pupils by a lenslet array and fed via optical fibers to the APDs, which do the photon counting. FlyEyes replaces the APDs with two CCID-35 CCD detectors and an SDSU2 controller. The optical fibers are removed from the APDs and rerouted to the CCID-35s. The CCID-35 detectors, conceived at ESO and MIT Lincoln Laboratory (MIT/LL), were specifically tailored for use in curvature wavefront sensing (Beletic et al. 2000; Dorn 2001). A block diagram of PUEO illustrating how the CCID-35s integrate into PUEO is shown in Figure 1. A more detailed explanation of the FlyEyes concept is given in Cuillandre et al. (2003) and Ho et al. (2004).

1.2. CCID-35

The CCID-35 device was developed by the European Southern Observatory (ESO) in collaboration with the MIT-Lincoln Labs fabrication facility (Beletic et al. 2000; Dorn 2001). One of its unique design features are storage areas on either side of the imaging array that are used to integrate charge from the intra-focal and extra-focal images used in curvature wavefront sensing. Having the storage areas eliminates the need to read out the images at each half cycle of the membrane mirror intra and extra-focal modulation (4 kHz in PUEO). The images can be clocked out at the full 1 kHz sampling rate, or at a lower divisor of 2 rate (e.g. 500 or 250 Hz) when observing faint guide stars.

The curvature sensing area of the CCID-35 consists of 8 columns nominally divided

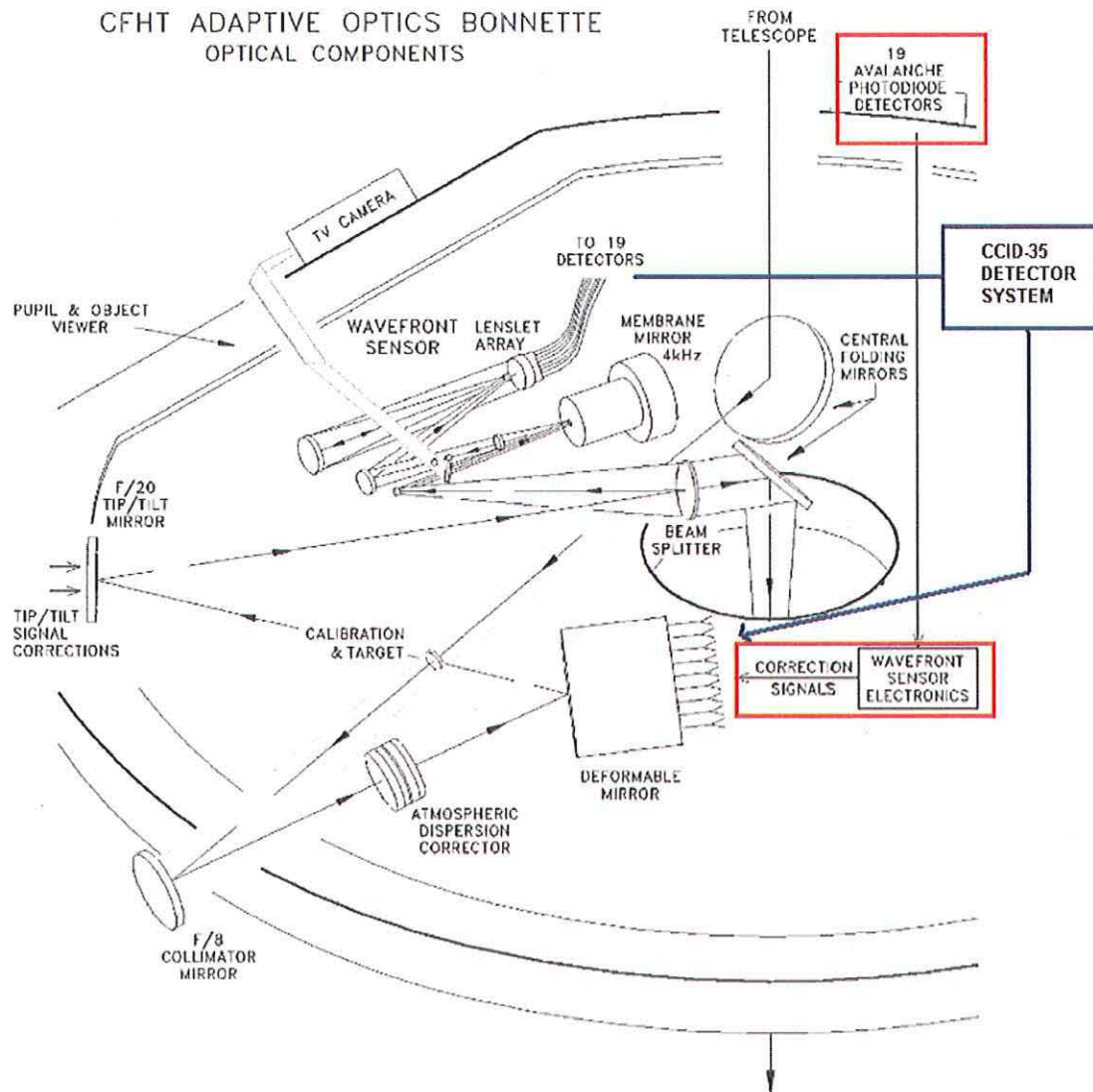


Fig. 1.— The APD and CCID-35 paths are shown in this diagram of PUEO. The fibers are disconnected from the APDs and connected to the CCID-35. Instead of the digitized sum and difference counters from the analog WFS electronics, the real time computer now receives values from a dedicated interface board.

into 10 cells, with an additional 8 cell column that can be used for tip/tilt sensing (not used in CFHT PUEO), Figure 2 (top). Nominally, each cell consists of a 20×20 pixel imaging area ($18 \times 18 \mu\text{m}$ sized pixels). Each column has its own serial output register and output amplifier allowing rapid readout of the array. Figure 2 (bottom) shows a diagram of the unit cell. Dorn and collaborators (?) found from simulations that the maximum acceptable read noise must be less than 2 electrons for the CCID-35 to provide a viable replacement for APDs. They successfully developed and tested a system at ESO with readout noise less than this value using front illuminated versions of these devices (Dorn 2001). These authors also The detectors are operated at -100°C . Dark current is not a concern given that exposure times are always less than 4 msec.

The device uses three-phase clocks for charge transfer. In figure 2, storage areas SA and SB store the charge for the half-cycle intra-focal (I) and extra-focal (E) images. The storage area SC is used to temporarily hold the charge as one half-cycle image is clocked out through the serial output register. Charge is binned into a super-pixel at the summing well before being output at the source follower amplifier.

The need for the storage area SC may not be immediately obvious as the output register could be used to store the charge to be read out. However, since there may in general be several intra/extra-focal cycles between each sampling of the intra/extra-focal signals, the storage register SC is required to store the A phase signal during completion of the readout of the previous B signal phase located in the output serial register.

2. FlyEyes Experiment

Originally designed for a high order curvature system with 104 subapertures, the wavefront sensor camera required two identical CCID-35 chips (since each one has 80

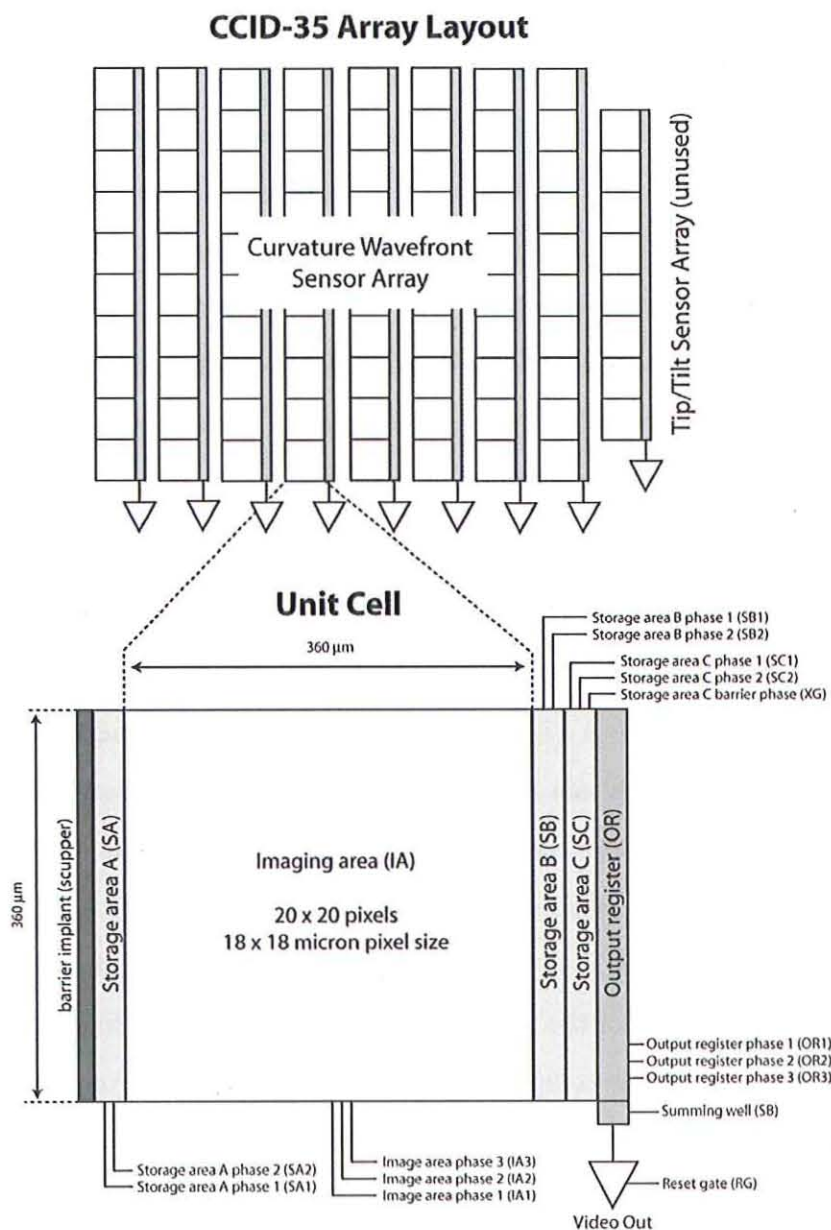


Fig. 2.— Architecture of the CCID-35 wavefront sensing CCD. Top: Array layout of 10x8 cells (“super-pixels”), plus the eight unused cells for tip-tilt sensing on the right. Bottom: unit cell, with the SA storage area on left and SB and SC storage areas on right of central integration area.

super-pixels) housed in a single dewar, fed by fibers, which suggested the name “FlyEyes”. Irrespective of the eventual outcome of the high order system, it was decided to compare this camera with the APDs to determine whether these detectors could compete with APDs in an operational environment. Therefore, the FlyEyes project was designed to use the existing software, hardware and interfaces, and to make no modifications to the existing hardware, such that the system could be restored to its original condition. Furthermore, the capability to switch between APDs and the CCID-35 so that side by side comparison testing could be done if not during the night, at least on consecutive nights, was deemed desirable. And of course, the base performance goal was to be able to maintain the current AO control loop performance (>80 Hz loop bandwidth at 1 kHz sample rate).

A picture of the system on the telescope is presented in Figure 3. Two CCID-35s are mounted in a liquid nitrogen cooled cryostat. Light from the lenslet array is brought into the cryostat via optical fibers. A SDSU2 controller from Astronomical Research Cameras, Inc. provides the clocks and biases for the CCDs. Four video processor boards with dual channels handle the amplification and digitization of the 8 video channels from the CCD (Only 19 cells – one for each subaperture of PUEO – distributed over 4 columns to use all the amplifiers are used in PUEO-FlyEyes). The SDSU2, which sits next to the cryostat mounted on the outside skin of the AO bonnette, transmits the readout data via fiber to the data acquisition PC in the computer room (roughly 70 meters from the telescope). A custom interface board ties in the existing interfaces to the SDSU2 controller and data acquisition PC. This board performs address and control signal multiplexing between the digital I/O board in the data acquisition PC and the existing wavefront sensor board (WFS). It also generates a synchronization signal from the 4 kHz clock which is used to synchronize timing patterns between the SDSU2 controller and the membrane mirror.

The data acquisition PC is a dual processor, 2 GHz machine running real-time Linux.

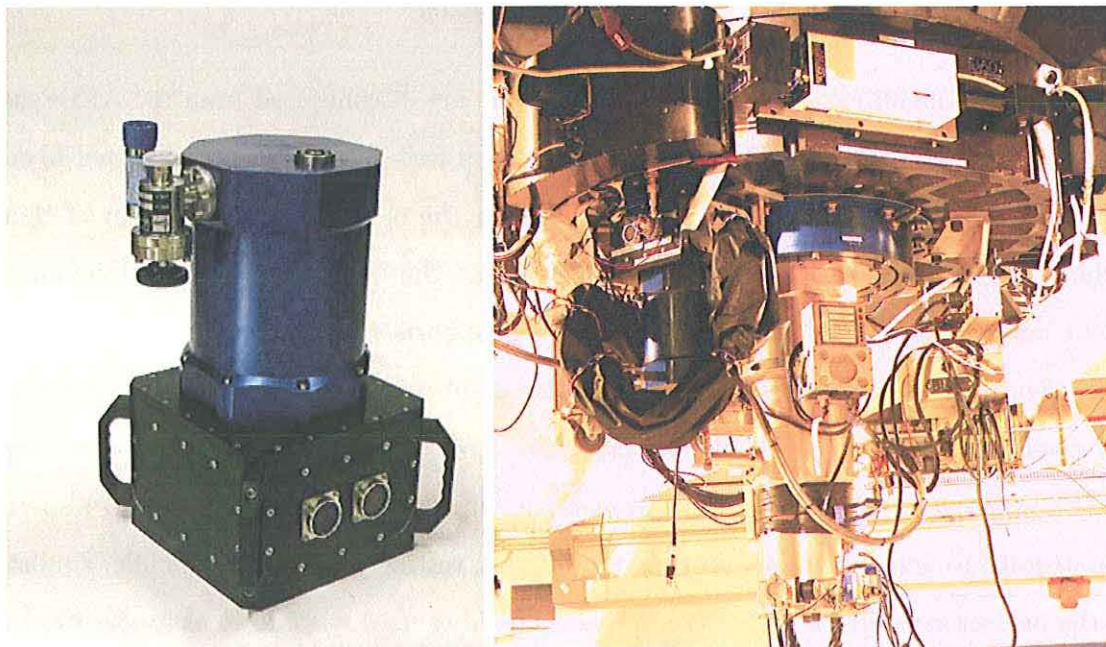


Fig. 3.— Left, FlyEyes dewar. Right, mounted on PUEO (black ring-like structure at top of picture) at the Cassegrain focus of CFHT; the gold dewar in the middle is the KIR scientific imaging camera.

The PC processes the readout data from the SDSU2, which are summed and differenced and then made available to the LaserDot real-time computer (RTC) through the custom interface board. The LaserDot RTC reads and normalizes the intensities, computes the control matrix and outputs actuator drive commands to the deformable mirror.

2.1. Fiber bundle

As briefly mentioned in Section 1.1, the fibers are disconnected from the APDs and rerouted to the CCID-35 cryostat through a vacuum feed-through flange. Internal fibers direct the light onto the CCID-35 detector. By far the most challenging aspect of the project was construction of the optical fiber bundle. The bundle required a minimum 19 fibers, one per each APD channel. The CCID-35 supports 80 fibers, one per each unit cell, much more than needed for PUEO. Building an 80-fiber bundle was deemed excessive for our needs so a 54-fiber bundle was settled upon. This 9x6 layout was largely determined by the V-grooves available to us but provided a sufficient number of spares and also an opportunity to gain experience in constructing and testing a large fiber bundle, similar to the one anticipated for a PUEO upgrade. The fiber used was identical to the 100 μm core diameter, low OH hydrogenated CeramOptec step-index fiber used to guide light to the APDs in PUEO. Two methods were considered in constructing the fiber bundle. Each involved precise positioning to match the center spacing of the unit cells, 360 μm x 560 μm . The first utilized silicon v-grooves blocks to form a fiber stack. V-grooves in the spacers were etched to match unit cell spacing, Figure 4, right. Ultimately the silicon v-groove method was chosen simply because the v-grooves had already been fabricated and were available.

Fixtures were developed to align and hold the fibers and v-grooves in place while bonding the fibers. Alignment of the individual silicon v-groove blocks proved to be very

difficult. The fiber bundle was aligned by registering the cleaved edges of the v-groove blocks. Unfortunately the cleaved edges were not identical or sufficiently consistent, which resulted in shifts in the fiber position from one row to the next. This offset can clearly be seen in the photograph of the bundle as well as the CCID-35 image of the light output from the individual fibers shown in Figure 5.

The second method consisted of epoxying fibers to a metal ferrule with an array of 145 μm holes spaced 360 μm x 550 μm , as shown on Figure 4, left. The metal ferrule approach would have provided a more precise fiber bundle and will be probably used should PUEO be upgraded. Electrical Discharge Machining (EDM) can easily produce a ferrule with an array of 145 μm conical holes at 360 μm x 550 μm spacing at relatively low cost.

The other challenge was positioning the fiber bundle above the CCID-35 surface to obtain a spot size that would fit within the unit cell while avoiding interference with the bond wires on the device. The fiber bundle had to be centered to within a few tens of microns in X, Y and θ had to be controlled for parallelism. An adjustment mechanism designed by GL Scientific using a two pairs of wedges provided for $\pm 700 \mu\text{m}$ in X and Y, and several degrees of rotation in θ . The height of the bundle above the face of the CCD (the Z direction) was fixed and mechanically set to 200 μm in the mount. There were no provisions for adjustment on the Z axis, although shims could be used to increase the spacing between the fiber bundle and surface of the CCID-35.

The fiber bundle was installed with the CCID-35 operating at room temperature in full frame imaging mode (e.g. Figure 5, right). Light was injected into the fibers and the CCD was read out in real-time to provide a streaming video image of the fiber spots. Since there was no way of knowing the alignment of the fiber bundle to the CCD other than through the CCD image itself, a fair amount of caution was used during initial installation. X, Y, and θ were controlled using the adjustment mechanism provided. Z was controlled using a

stack of shims that were removed, one at a time, to lower the fiber bundle toward the face of the CCD in a controlled fashion.

In the end the height of the bundle above the CCD face was close to the $183\text{ }\mu\text{m}$ estimated and the spots were fairly well centered in the unit cells. During alignment the bundle was removed and installed several times with no apparent shift along any axis. The adjustment mechanism performed well and has been stable after more than 10 cooling and warming cycles. No adjustments have been made since the initial alignment.

One drawback in the design of the fiber bundle was the vacuum feed-through. By necessity, bare fibers had to be used in vacuum and jacketed fibers outside the cryostat. This made for a fiber bundle with a very heavy and fragile end. Several fibers were broken during fabrication and installation because of this. The missing spots in Figure 5 indicate the location of the broken or poor transmission fibers.

2.2. Interface patch board

A simple interface board was designed to receive the intra-focal and extra-focal data from the SDSU2 controller and format it for the LaserDot RTC. Previously the WFS handled these tasks. The design was driven by the constraints of the project, namely, that the current software and hardware interfaces had to be maintained and no modifications to the existing hardware could be made.

In the original PUEO design, the intra-focal (I) and extra-focal (E) pulses from the APDs clock a multiplex of 38 (19 APDs \times 2) 16-bit up-down counters. Discrete logic would combine the I and E pulses into the sum ($I + E$), and difference ($I - E$), signals. The sum and difference signals would each clock an individual counter. The output of the counters would be latched and stored in registers on every sampling period (e.g. at 1 kHz). The

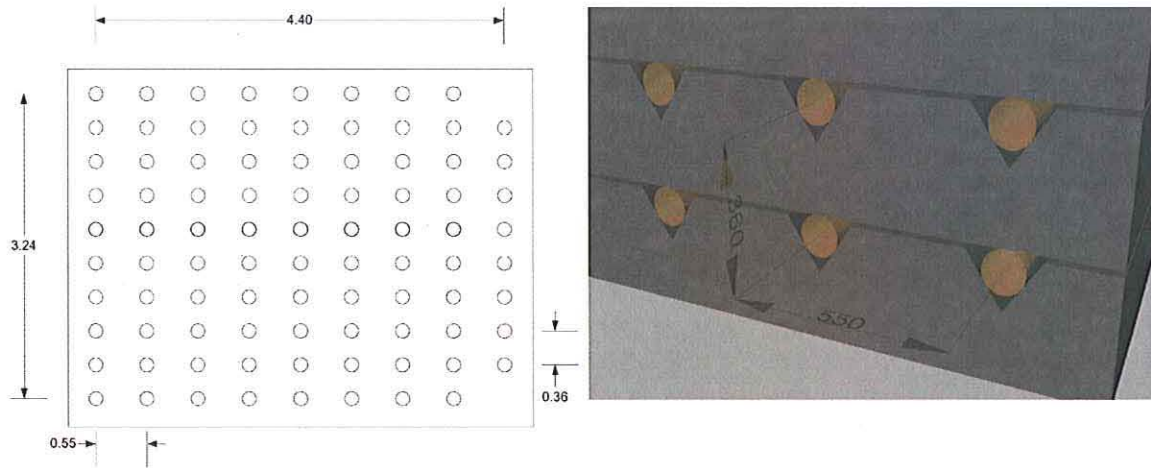


Fig. 4.— Left, Ferrule hole pattern (dimensions in mm); this method would have provided a more precise fiber bundle. Right, illustration of the stacked silicon v-groove spacers. These ended being used because they had already been fabricated and were available.

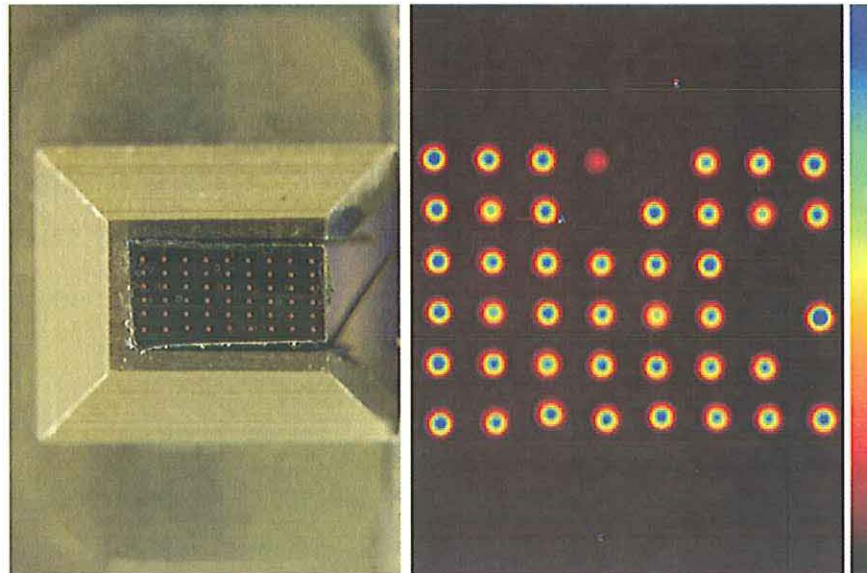


Fig. 5.— Left: End view of fibers, 9x6 fiber bundle epoxied into mounting fixture. Right: Afocal image of the 8x6 fiber output on the CCID-35, without the tip-tilt columns. Note that the image includes 20 pixels of over-scan on the top edge (normally used for noise analysis). Broken or poor transmission fibers can be seen on the top and right sides.

LaserDot RTC addresses and reads the sums and differences for each APD in nineteen 32-bit reads and uses these to compute the drive signal to the deformable mirror.

In the new interface board, I and E data from the SDSU2 controller is transmitted down a single fiber and is converted into 2 parallel words using a HOTlink receiver/converter pair. The data words are written into a FIFO and then stored in a 32K x 8 SRAM. I and E data from 64 of 80 unit cells of the CCID35 are read regardless of whether they are illuminated with light from the fibers or not, in order to maintain consistent timing between the sampling of different cells. During the commissioning, all the operational fiber and unit cell pairs were examined by viewing the spot image and the optimal 19 were selected. An address decoder implemented with a complex programmable logic device (CPLD) maps the locations of the best 19 fiber spots to the original LaserDot addresses. By necessity the interface board uses the same input and output signals and definitions as the WFS. A pair can easily be changed if needed, for instance if its fiber got broken, by simply remapping the LaserDot RTC addresses to the addresses corresponding to the new pair. This is done through a JTAG port and CPLD programming software. Unlike in the original WFS, the I and E sums and differences are not available, only the raw data. The LaserDot RTC addresses and reads the I and E data and computes the sums and differences in the real-time code.

If PUEO were to be upgraded with FlyEyes, all the electronics and RTC would be redesigned. The present hardware is obsolete and non-scalable. The scheme used on the interface board would not be considered since it was designed simply to interface with the present hardware. The hardware required would conceivably be much simpler than what was necessary to integrate FlyEyes with PUEO.

2.3. CCID-35 WFS camera

An image of the fibers on the CCD is shown in Figure 5. Several fibers are broken and a few CCD cells are unusable due to defect structures. For PUEO, only 19 channels are needed so this does not present a problem. The fibers selected for the signals were from the fibers in the 3 cell rows nearest the output amplifiers to minimize the time required to shift out the pixels.

In CFHT’s PUEO instrument, the membrane mirror cycles between the intra-focal (I) and extra-focal (E) images at 4 kHz, however the readout of the photon counts associated with each phase is performed at 1 kHz in its highest bandwidth operation mode. When the avalanche photodiodes (APDs) are used for sensing, the system alternates 4 times per 1 kHz cycle between incrementing the I or E counters. If the sensing frequency is reduced by n octaves, then the system must alternate 4×2^n times between feeding the I or E counters before these are read out. The CCID-35 is clocked in such a way as to emulate this behavior. The readout of the CCID-35 is performed as quickly as possible, within the limits necessary for maintaining low readout noise, in order to minimize the phase-lag between the readout of the intra-focal and extra-focal signals.

The unbinned readout noise for this device was previously reported by Ho et al. (2006). Further tests using an alternate measurement method confirmed these results, however it was found that the noise was significantly higher when binning the pixels 20×20 in AO mode compared to the unbinned, imaging mode. It was found that the noise could be significantly reduced (from 3, down to 2 electrons RMS) by limiting the swing of the parallel and serial clocks. The most likely explanation for the excess noise at the higher clock swings is spurious charge generation through impact ionization. Although the probability of generating charge in this manner is usually negligibly small at such small voltage swings, the large number of shifts (and fast clock edges) used when operating the

device in AO mode (over 80 when sampling at 1 kHz) could lead to a significant effect. A noise transfer curve for one channel of the CCD operated in AO mode is shown in Figure 6. The readout noise obtained ranged from 1.9 to 2.7 e^- RMS, with an average noise of 2.3 e^- RMS.

3. Expected performance and simulations

Although early simulations (Craven-Bartle et al. 2000) show that the performance of FlyEyes should be equivalent to that of the APDs, the read-noise of a CCD introduces changes in the operation of a curvature wavefront sensor.

3.1. Read noise

In photon counting detectors, the noise on the wavefront sensor measurements is integrated in the servo-loop and low frequencies are more strongly attenuated due to their improved SNR. Thus with APDs, the noise (i.e. the variance of the wavefront sensor signal per integration cycle) goes as N^{-1} with N the number of photons detected in a sample time. In a CCD on the other hand, read noise is added in every frame so the noise goes as N^{-2} , where the N photons have now been detected in one read, see e.g. Rousset (1999). This is shown in Figure 7, which shows the noise (and Strehl attenuation) for photon and read noise limited wavefront sensors; in a real sensor, the photon noise is added to the read noise, but we neglect this effect as we only focus on the dominant source of noise in each measurement.

The following equation can be used to calculate the WFS measurement variance for the APDs where the photon noise dominates (see e.g. Rousset (1999). eqn. 5.45 & Rigaut

et al. (1998), eqn.1).

$$\sigma_{WFS}^2 \simeq \frac{\pi^2}{\eta \times QE_{APD} \times N_{photon}} (rad^2) \quad (1)$$

where η describes the throughput (and wavefront sensor sensitivity), N_{photon} is the number of photons per integration time, and QE_{APD} is the APD quantum efficiency, 0.35 in this case; to reproduce PUEO’s behavior (see e.g. Rigaut et al. (1998), figure 9), we set η to 0.16; this provides the proper Strehl attenuation (50% at magnitude 15.7), as measured experimentally. For the CCID-35, we can derive the WFS measurement variance from Rousset (1999), eqns. 5.46, 5.42 and 5.43, as:

$$\sigma_{WFS}^2 = \pi^2 \frac{(\sigma_{read} \times n_{pixels})^2}{(\eta \times QE_{CCD} \times N_{photon})^2} + \sigma_{bandwidth}^2 \quad (rad^2) \quad (2)$$

where the read noise per pixel σ_{read} is $2.3 e^-$, read over n_{pixels} (we assume 2, one for the intrafocal read, the other for the extrafocal one), where N_{photon} is the number of photons per unit time, and QE_{CCD} is the CCID-35 quantum efficiency, assumed to be 0.9. We neglect the photon noise term which only becomes dominant at very high photon flux and the last term, $\sigma_{bandwidth}^2$ is the phase lag error. This term is required because although increasing the integration time on the WFS improves the SNR in terms of detected photons, it does so at the expense of the temporal error, determined by the Greenwood frequency and the loop correction frequency. In the example shown in Figure 7, the CCID-35 is operated at 1 kHz with no phase lag error, at 500 Hz (double the number of photons per exposure) but with a $0.2 rad^2$ phase lag error and at 250 Hz with a $0.9 rad^2$ phase lag error. This figure illustrates that on the bright end, the improvement in QE allows to improve the performance with respect to APDs, while at the faint end where the read noise starts to dominate, the APD performance level can be emulated by lowering the sampling frequency: the performance at 500Hz becomes better than at 1kHz at magnitude 14, and it improves again by going to 250Hz around magnitude 16. The above formulas make no assumptions as to the exact form of the noise, but compare simple, empirical models with the same constants so these results

strongly imply that by carefully adjusting the wavefront sensor frequency, the performance of the APDs on PUEO can be matched when using the CCID-35.

3.2. Low flux levels

Another difference introduced by the finite read noise of the CCD appears at very low flux levels. The wavefront sensor estimates the local wavefront curvature by estimating the contrast between the intra/extra-focal images:

$$C = \frac{I_{intra} - I_{extra}}{I_{intra} + I_{extra}} \propto \nabla^2 \phi \quad (3)$$

In the absence of read noise, the denominator can only be zero when the numerator is also zero, and so if no photons are detected during an integration cycle, we set C to zero. But in the presence of read noise, the denominator can be null or negative once the bias level has been subtracted out (it turns out to be less of a problem if it is negative rather than null). Various schemes were simulated to try to reduce the instability and improve poor performance at low flux. These included: clipping the denominator to positive values only, using a running average on the denominator and adding a bias to the detected intensities. Results of Monte Carlo simulations using the IDL code `simul.pro` developed by François Rigaut (private communication) are presented in Figure 8.

Clipping the denominator made the loop unstable and was not pursued. It is apparent that a running average in the denominator only marginally improves the performance, if at all. Adding a bias seems to have a more important effect: the bias subtracts out in the numerator, but adds a constant term in the denominator, effectively lowering the loop (or integrator) gain. As all the simulations were run with a constant loop gain of 0.6, adding a bias to the detector signal improves the results of the simulations at low photon flux. However, PUEO uses a modal control that self-optimizes in closed loop and applies the gain

that reduces the residual phase variance. Therefore when this method was tried on the sky, it was not found to improve performance.

Sky testing revealed that the detailed modeling presented above, which should have predicted the optimal wavefront sensing frequency as a function of the guide star brightness, did not take into account the varying sky conditions. Even accounting for r_0 fluctuations did not allow us to definitively and repeatedly demonstrate an improvement of performance on faint sources at lower sampling frequencies. This may have been due to a rapidly varying atmospheric conditions or very short correlation times, τ_0 .

4. On-sky performance

FlyEyes was tested on PUEO on the nights of April 24th-26th 2007 on bright guide stars, on February 25th-27th 2008 over a range of guide star brightness and a comparison run with the APDs took place on December 17th-18th 2007. The comparison tests indicate that the bright star performance is unaffected, as shown in Figure 9. It shows the delivered Strehl ratio as a function of the r_0 (in cm) at the wavelength of observation. The black crosses show the original 1996 integration data, which consisted of more than 300 observations of stars at all wavelengths in varying conditions (Rigaut et al. 1998). The red diamonds show the dynamic Strehl ratio measured on images obtained with KIR (the science camera) in April 2007 as a function of the r_0 estimated from the wavefront sensor data and they lie right at the expected value. Experiments with the various schemes described in section 3.2 were carried out but it was found that the loop remained most stable with no modifications (i.e. no bias nor running average).

The comparison with APDs turned out to be more difficult than anticipated due to varying seeing (and τ_0) conditions, leading to a very large spread of performance for a given

magnitude. Nonetheless, by recording and correcting for the r_0 estimated by the wavefront sensor data during the February 2008 observing run and comparing it to our model and the original 1996 integration data, we were able to confirm that the performance was not noticeably degraded by using FlyEyes instead of the APDs. Images of the guide stars were simultaneously recorded in K-band on the KIR infrared camera, and standard data reduction techniques were applied to extract the PSF and measure the Strehl ratio.

The modal control of PUEO works by estimating the input phase power spectrum from measuring the residual power spectrum of the WFS measurement and using a model of its well-known and characterized closed loop transfer function. Once the input spectrum is estimated, the loop gain which minimizes the integral of the product of this spectrum multiplied by the associated error transfer function is determined. This gain applied to the loop and the whole process is repeated; the loop gain thus self-optimizes in closed loop. This process depends on the transfer function used, and in PUEO, the temporal characteristics of the integrator and the photon noise make this a straightforward process. We were unable to implement a full modal control for FlyEyes as the closed loop transfer function associated with this detector was unknown and it would have required modeling (or measuring) the transfer functions and the read noise for the different sampling frequencies and loop gains with little certainty in their accuracy. Instead, we ran our tests with either the modal control enabled (assuming the simplest loop integrator, but neglecting read noise, thus probably not optimized) or with zonal control enabled, setting the gain manually. This made the testing cumbersome, but a sufficient number of data points were collected to see trends emerging, as shown in Figure 10.

The top row shows the number of detected photons translated into magnitudes as a function of the quoted guide star magnitude. Some spread can thus be expected due to varying spectral type and photometric conditions. The zero point of 18.5 is the same for

FlyEyes as it is for the APDs (Rigaut et al. 1998). The black \times symbols are for 1 kHz data, the lighter $+$ symbols for 500 Hz and the light \diamond for 250 Hz. Note the read noise seems to appear at magnitude 15.4 at 1 kHz.

The middle row shows the raw K-band Strehl ratio, as measured on the KIR detector as a function of the guide star magnitude. The spread is understandable as there is no accounting for either the actual detected number of photons or the r_0 at the time of the observations. The left panel shows modal control and the right panel shows zonal control; and as above, in both cases the black \times symbols represent the 1 kHz sampling frequency, the lighter $+$ symbols show 500 Hz, and the light \diamond 250 Hz. The spread is such that it is hard to infer any quantitative assessment of the performance, although qualitatively, it would appear that lowering the sampling frequency ought to improve the performance above magnitude 11. This is misleading however, as the 1kHz performance is much lower than the expected 60% that PUEO routinely delivers on bright stars in K band (e.g. figure 9). To be comparable, these data points have to be corrected for the Strehl attenuation due to the instantaneous r_0 . This is achieved by using a fit of the Strehl attenuation as a function of r_0 (as in figure 9).

The bottom row shows the final result, after having accounted for the static Strehl ratio, the number of detected photons and r_0 at the time of the observations. The small black dots are the dynamic (i.e. corrected only for static aberrations) Strehl at 1 KHz, leaving the spread unchanged, but renormalized. The black \times symbols show the same data corrected for r_0 , and can thus be interpreted as the Strehl ratio attenuation. The lighter $+$ show the Strehl attenuation at 500 Hz and the light \diamond symbols at 250 Hz; the spread of the data is reduced. A best-fit model to the data is shown by the curves (the dashed curves show by how much the 1 kHz curve would be displaced if halving the sampling frequency simply doubled the number of photons, assuming a negligible phase lag error). There is a

fair agreement especially for the 250 Hz data at the faint end. Also note that on bright (magnitude 12) stars, the zonal control performs much more poorly at 500 and 250Hz than at 1 kHz, as was expected (e.g. Figure 7). However, in modal control at high flux, the read noise is small compared to the photon and lag noise, so the loop gain optimizing algorithm seems to be doing the right thing, improving the performance by increasing the loop gain so as to compensate the lower loop frequency. Quantitatively, we can point out that we expect a Strehl attenuation of 50% due to the guide star brightness at around magnitude 15.

A direct comparison with the APDs performance was not possible due to the poor seeing and high variability of τ_0 at the time of observations. However, since PUEO’s behavior is well understood, the comparison to the model established in section 3.1 is presented in Figure 11. To fit the 250Hz and 500Hz data on faint magnitudes, the throughput and wavefront sensor sensitivity factor η had to be decreased from 0.16 to 0.10, which decreases the APDs 50% Strehl attenuation from magnitude 15.7 to 15.2. This leads to a slight overestimation of the performance (for both the FlyEyes and APD curves) around magnitudes 10 to 12 although as we have seen, the 1kHz FlyEyes correction shown on the middle panels of figure 10 and expected to be around at least 60% in K band, produces Strehl ratios on the order 30% to 40%. r_0 was measured to be around 10cm at the time of these observations and it is thus likely that this poor seeing is partly responsible for the poor performance at these medium magnitudes. This discrepancy can also be due to poorly tuned zonal loop gain, as is shown by the modal control points at 1kHz which all lie very close to the expected curve (with $\eta=0.10$). It is not clear why η should be different with the APDs, although we do expect extra losses in throughput due to the extra length of fiber and the extra connector used in FlyEyes. We developed a new fiber bundle to be used with the APDs that replicated the FlyEyes fiber bundle (with an extra connector and extra fiber length) but the quality of the data acquired with the APDs was not good enough to allow a direct comparison and determine η independently. Besides the expected

connector losses, it is also possible that the throughput of PUEO has decreased over the 14 years since commissioning. What is important for our purposes is that the same value for η is used in the comparison between the APDs and FlyEyes.

The values for $\sigma_{bandwidth}$ are very roughly estimated at 0.65 rad^2 for 500Hz and 0.8 rad^2 at 250Hz, although these values are expected to be highly dependent on τ_0 and the wavefront sensor estimation of r_0 . These values will also have a large effect on the sampling frequency crossover magnitudes, which our data is not quite accurate enough to resolve, but we do find that reducing the sampling to 500 Hz at around magnitude 15 and to 250Hz at magnitude 16 improves the performance with respect to 1kHz, roughly as expected from figure 7 and allows to regain the APDs performance, which shown by the dotted line on figure 11. FlyEyes provided a (measured) Strehl ratio of 25% at 250Hz on a magnitude 15.8 star for a short period.

Even though a direct comparison to the APDs was not possible, these FlyEyes results are at least as good as the model of our APDs from commissioning data if we assume the same throughput η for both. This conclusively demonstrates that a CCD based detector can successfully be used to replace APDs in curvature sensing and although the decreased demand on PUEO implies that there is no immediate motivation to do so, FlyEyes is ready to be integrated to PUEO. An upgrade of PUEO is now easily within reach, should the astronomical community support it.

5. Conclusion

We have described the FlyEyes experiment, which used a CCID-35 CCD detector as an alternate detector to PUEOs APDs. The CCID-35 has better quantum efficiency than the passively quenched APDs used in PUEO, but introduces a $2 e^-$ read noise penalty.

FlyEyes was successfully integrated and tested with PUEO using a fiber bundle to divert the light from the APDs to a CCID-35 detector. An interface board was implemented to send the WFS measurements to the Real Time Computer. On-sky operation was achieved on bright stars ($V < 10$). On fainter stars ($10 < V < 16$), different schemes were attempted to reduce the effects of the read noise, but none showed definitive improvements under our test conditions. FlyEyes performed at least as well as APDs, although varying atmospheric conditions made the task of establishing performance as a function of guide star magnitude difficult. Quantitatively, a Strehl attenuation of 50% can be expected when the guide star is magnitude 15; this is also the crossover frequency where 500Hz improves the performance with respect to 1KHz. At around magnitude 16, decreasing the sampling frequency to 250Hz improves the correction again. Anecdotally, FlyEyes provided 25% Strehl ratio on a 15.8 magnitude star. The demand for PUEO is steady but low, so there is no strong incentive to use FlyEyes as a replacement for the APDs as this would require further effort into integrating FlyEyes into PUEO and improving the reliability and automation of the performance optimization. However, an upgrade of PUEO is now within reach: Curvature AO systems with 100~200 subapertures are now operating with spectacular success, and the results presented in this paper show that it is now possible to reduce their cost substantially by replacing the APDs with CCDs.

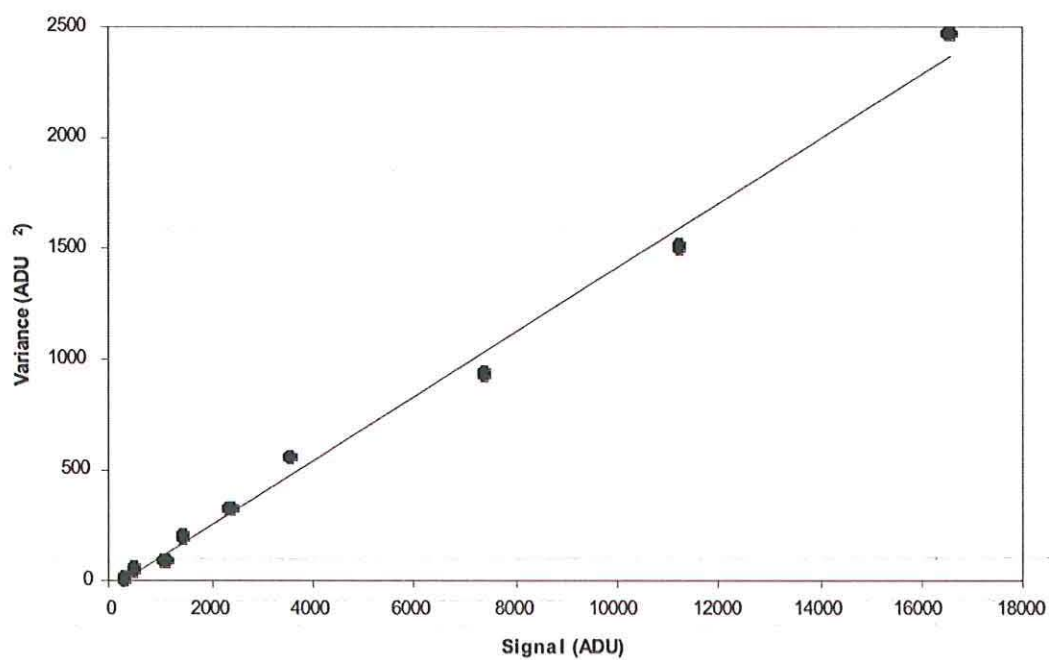


Fig. 6.— Noise transfer curve for one channel of the CCID-35 operated in AO mode with 1 kHz sampling. The average read noise for the array was $2.3e^-$.

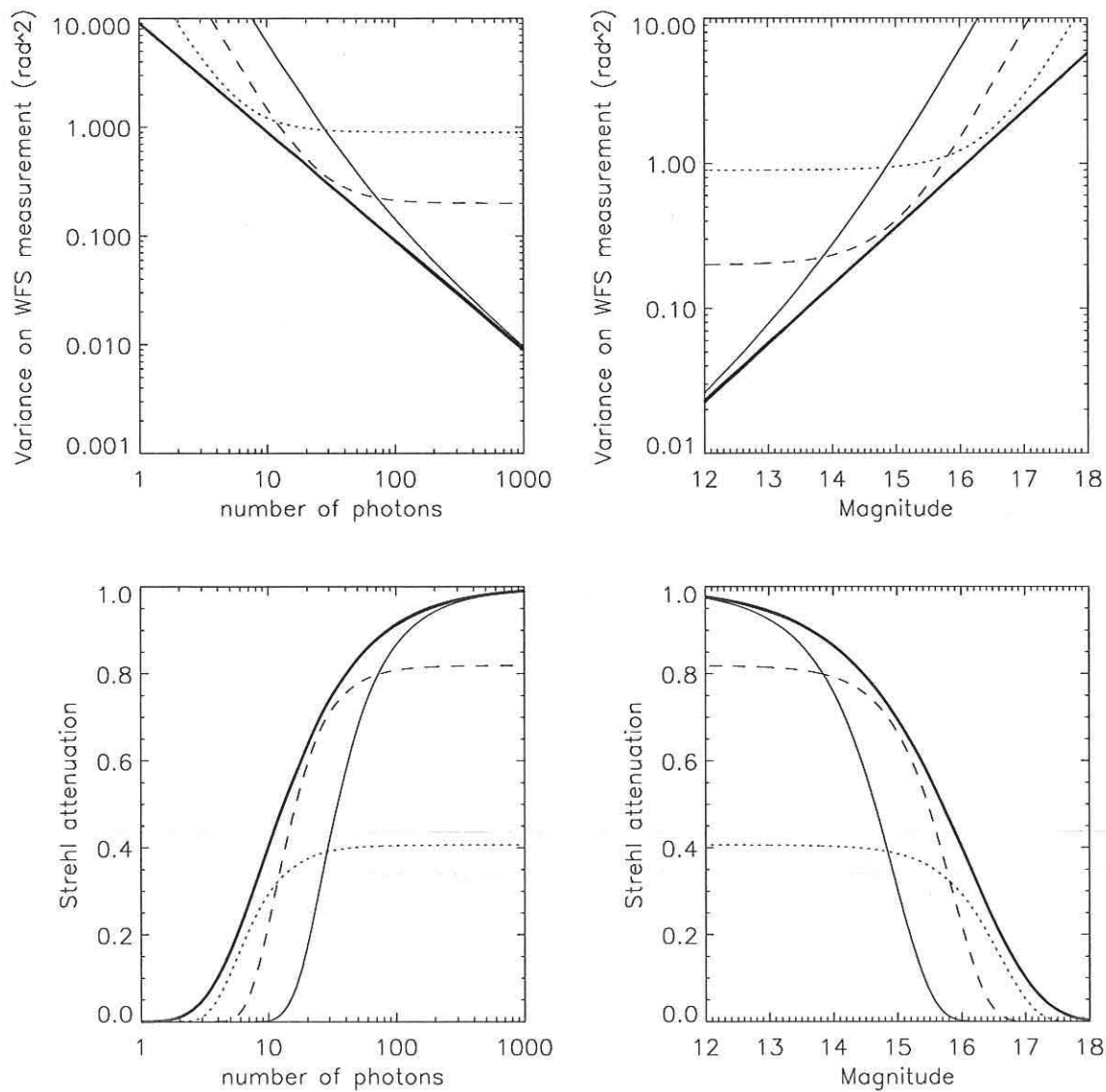


Fig. 7.— Computed variance on WFS measurements (top) and equivalent Strehl attenuation (bottom) for incident number of photons (left) and equivalent Guide Star magnitude (right) for APDs (i.e. photon noise only, bold line) and CCID-35 (including read noise, 1kHz: full line, 500Hz: dashed line, 250Hz: dotted line).

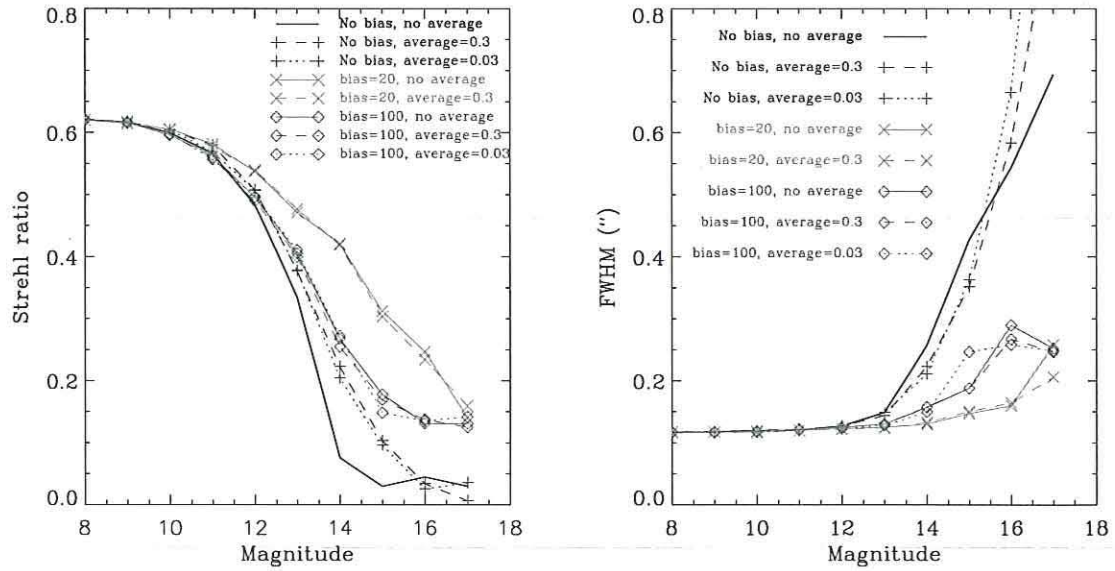


Fig. 8.— Simulated Strehl and FWHM as a function of guide star magnitude, with bias or running average in denominator to prevent loop instabilities. A bias of 20 seems to provide the most improvement in this case.

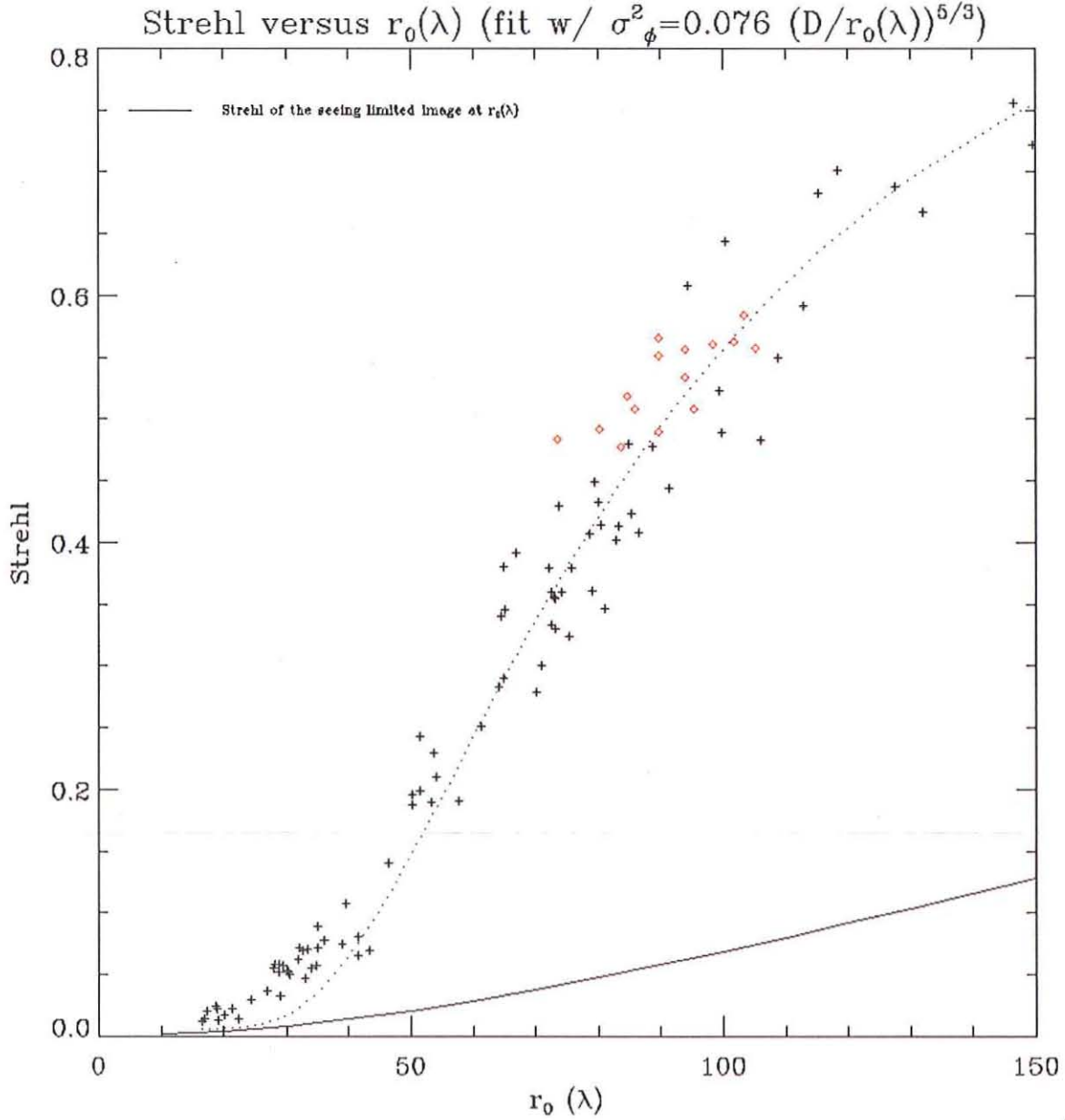


Fig. 9.— Bright guide star performance, showing the delivered Strehl ratio as a function of r_0 expressed in centimeters at the wavelength at which the Strehl ratio is measured (λ); original 1996 integration data, black crosses, April 2007 data, red diamonds. The performance is unaffected by FlyEyes.

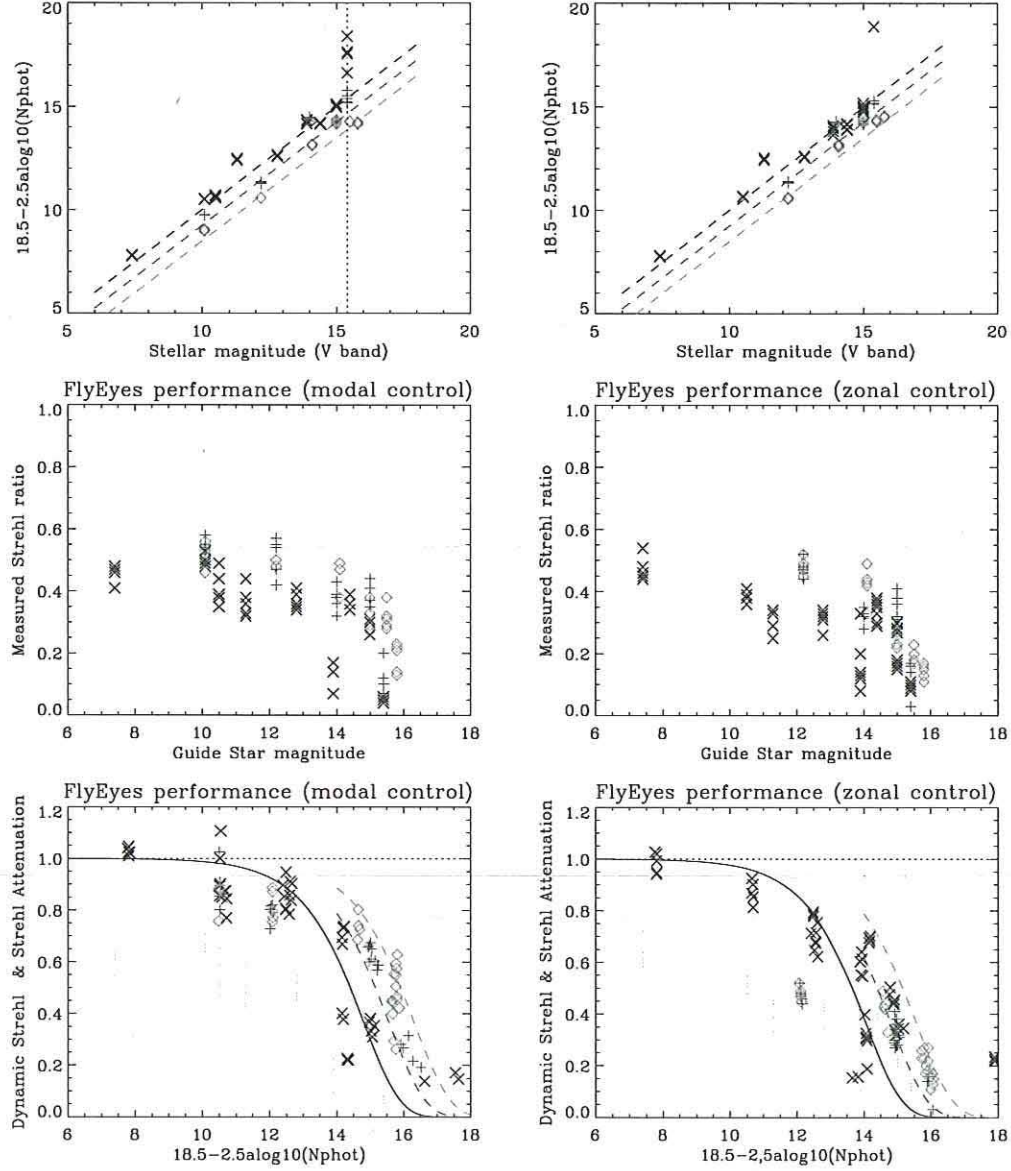


Fig. 10.— FlyEyes performance as a function of guide star magnitude. left column is with PUEO modal control, while the right one is for zonal control at various gains. Top row: photometry. Center, measured Strehl ratio on IR camera. Bottom: Strehl attenuation, corrected for r_0 . 1kHz: black \times , 500Hz: gray $+$, 250Hz: light gray \diamond - see text for details.

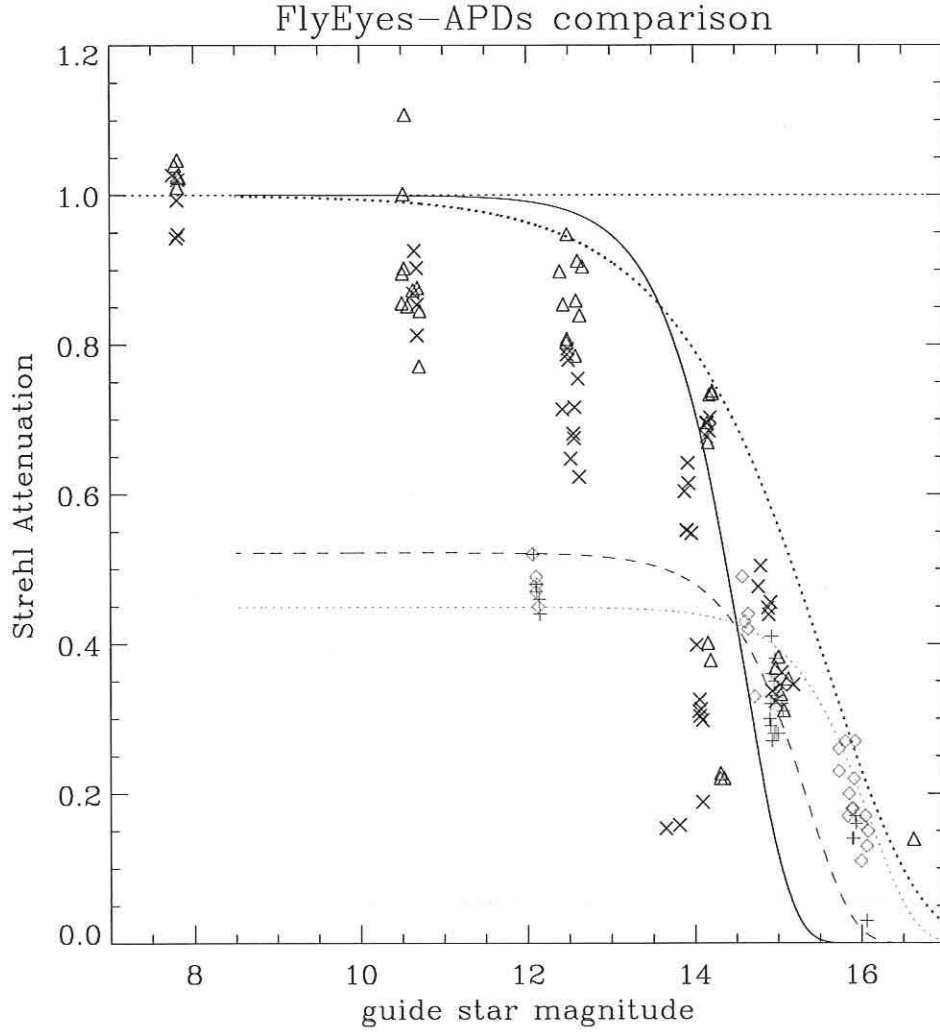


Fig. 11.— Comparison of FlyEyes modal (1kHz: black \triangle) and zonal control performance (1kHz: black \times , 500Hz: gray $+$, 250Hz: light grey \diamond) as a function of guide star magnitude compared to APDs model from Figure 7. Full line: FlyEyes model, lighter dashed: FlyEyes 500Hz model, light dotted: FlyEyes 250Hz model; black dotted line: PUEO APDs model, with $\eta=0.10$. The discrepancy around magnitude 10~12 can be attributed to a poorly tuned loop or very fast atmosphere, but the critical crossover behavior occurs between magnitudes 14 and 16.

REFERENCES

- Beletic, J.W., Dorn, R.J., Craven-Bartle, T., Burke, B., “A new CCD designed for curvature wavefront sensing”, 2000, *Optical Detectors for Astronomy II: State-of-the-Art at the Turn of the Millenium. 4th ESO CCD Workshop*.
- Craven-Bartle, T.V., Dorn, R.J., Beletic, J.W., “Computer simulation comparison of CCDs and APDs for curvature wavefront sensing”, 2000, *Proc. SPIE* **4007**, 444.
- Cuillandre, J.-C., Beletic, J.W., Dorn R.J., Luppino, G.A., Isani, S., Gorceix, N., Lai, O., Craven-Bartle, T.V., Burke, B.E., Mnard, F., “FlyEyes: a dual CCD detector system for CFHT PUEO NUI’s wavefront sensor”, 2003, *Proc SPIE* **4839**, 272.
- Dorn, Reinhold J., “A CCD based curvature wavefront sensor for adaptive optics in astronomy”, 2001, *Ph.D. dissertation*, Ruperto-Carola University of Heidelberg, Germany.
- Ho, K., Cuillandre, J.-C., Puget, P., Salmon, D., Lai, O., Beletic, J.W., Luppino, G., Dorn, R., J.; Burke, B., “Update report on FlyEyes: a dual CCD detector system upgrade for PUEO”, 2004, *Proc SPIE* **5499**, 395.
- Ho, K. J., Cuillandre, J.C., Lin, C.J., Benedict, T., Lai, O., Ward, J., Salmon, D., Luppino, G., Beletic, J., Dorn, R., Puget, P., Burke, B., Wang, S.Y., “FlyEyes: Integrating CCID-35 into PUEO AO system at CFHT”, 2006, *Proc. SPIE* **6276**, 62761G.
- Lai, O. , Ménard, F., Cuillandre, J.-C., “PUEO NUI: feasible and fast upgrade of the CFHT Adaptive Optics system for high dynamic range imaging”, 2003, *Proc SPIE* **4839**, 659.
- Lai, O., “Sawn song for an Owl: the scientific cases for Pueo Nui eProceedings”, 2004. *eProceedings CD Rom of Grenoble Workshop*. Editor: O Lai.

- Racine, R., “The Strehl Efficiency of Adaptive Optics Systems”, 2006, *Publ. Astron. Soc. Pacific*, **118**, 1066.
- Rigaut, F.J., Salmon, D.S., Arsenault R.A., Thomas, J., Lai, O., Rouan D., Véran J.-P., Gigan, P., Crampton, D., Fletcher, J.M., Stilburn, J., Boyer, C. and Jagourel, P., “Performance of the Canada-France-Hawaii Telescope Adaptive Optics Bonnette”, 1998, *Publ. Astron. Soc. Pacific* **110**, 152.
- Rousset, G., “Wavefront Sensors” in *Adaptive Optics in Astronomy*, 1999, F. Roddier, editor.